

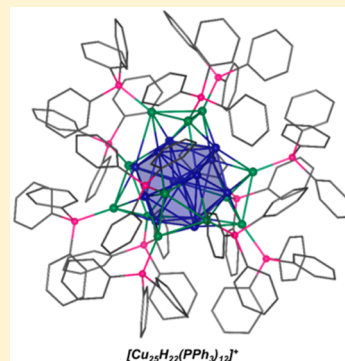
A Cu₂₅ Nanocluster with Partial Cu(0) Character

Thuy-Ai D. Nguyen,[†] Zachary R. Jones,[†] Bryan R. Goldsmith,[‡] William R. Buratto,[†] Guang Wu,[†] Susannah L. Scott,^{*,†,‡} and Trevor W. Hayton^{*,†}

[†]Department of Chemistry & Biochemistry, and [‡]Department of Chemical Engineering, University of California, Santa Barbara, California 93106, United States

S Supporting Information

ABSTRACT: Atomically precise copper nanoclusters (NCs) are of immense interest for a variety of applications, but have remained elusive. Herein, we report the isolation of a copper NC, [Cu₂₅H₂₂(PPh₃)₁₂]Cl (**1**), from the reaction of Cu(OAc) and CuCl with Ph₂SiH₂, in the presence of PPh₃. Complex **1** has been fully characterized, including analysis by X-ray crystallography, XANES, and XPS. In the solid state, complex **1** is constructed around a Cu₁₃ centered-icosahedron and formally features partial Cu(0) character. XANES of **1** reveals a Cu K-edge at 8979.6 eV, intermediate between the edge energies of Cu(0) and Cu(I), confirming our oxidation state assignment. This assignment is further corroborated by determination of the Auger parameter for **1**, which also falls between those recorded for Cu(0) and Cu(I).



INTRODUCTION

Atomically precise, noble metal nanoclusters (NCs) are a relatively new class of materials, with potential applications in catalysis, medicine, and imaging.^{1–7} Many examples are now known, including [Ag₄₄(*p*-MBA)₃₀]^{4–}, [Ag₂₁(S₂P(O^{*i*}Pr)₂)₁₂]⁺, [Au₂₅(SCH₂CH₂Ph)₁₈][–],^{10,11} and [Au₁₀₂(*p*-MBA)₄₄].^{12,13} Intermetallic Au_{*m*}Ag_{*n*} and Au_{*m*}Cu_{*n*} nanoclusters are also isolable.^{14–19} Significantly, their monodisperse and atomically precise nature has permitted their complete structural characterization, allowing for the development of structure/function relationships for these nanomaterials.^{20–23} NCs have also proven to be an excellent testbed for superatom theory, helping to place it upon firm experimental footing.²⁴

In contrast, comparable copper NCs have remained elusive. Previous attempts to generate large Cu NCs have produced ill-defined mixtures,^{25–28} or required the use of cryogenic matrices.^{29,30} Interestingly, several well-defined Cu(I) hydride clusters are known, such as [Cu₁₄H₁₂(phen)₆(PPh₃)₄]²⁺,³¹ [Cu₁₈H₇(1,2-S(C₆H₄)PPh₂)₁₀(I)],³² [Cu₂₀H₁₁(S₂P(O^{*i*}Pr)₂)₉],^{33,34} [Cu₂₈H₁₅(S₂CN^{*n*}Pr₂)₁₂]⁺,³⁵ and [Cu₃₂H₂₀(S₂P(O^{*i*}Pr)₂)₁₂],³⁶ but these complexes do not feature any Cu(0) character. Indeed, even Cu(0) coordination complexes are exceptionally rare.^{37–40} Relative to the heavier congeners, the enhanced challenge of generating Cu(0) nanoclusters is due, in part, to the lower M(I)/M(0) half-cell potential of Cu (0.52 V) versus Ag (0.80 V) and Au (1.69 V).⁴¹ As a consequence, the Cu(I) monomers formed prior to NC aggregation are more resistant to reduction. It also renders any resulting Cu(0) NCs more air-sensitive, which makes their physical isolation more challenging. Despite these challenges, Cu nanomaterials are of intense interest for a variety of catalytic applications, including the electrochemical reduction of CO₂.^{42–46} In this regard, the

isolation of atomically precise copper nanoclusters would be a significant advance, because they could help address the unanswered mechanistic questions that remain for this transformation.^{47,48} Herein, we describe the synthesis and structural characterization of a novel Cu₂₅ nanocluster that features a Cu₁₃ centered-icosahedral core, and probe its electronic structure with X-ray absorption spectroscopy (XAS) and X-ray photoelectron spectroscopy (XPS).

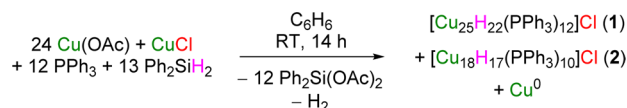
RESULTS AND DISCUSSION

As mentioned above, Cu(I) is more resistant to reduction than either Ag(I) or Au(I). As a result, reduction of a Cu(I) precursor with a hydride source, a common way of making Ag and Au NCs, often only results in the synthesis of stable Cu(I) hydride clusters.^{49,50} For example, reduction of Cu(OAc)₂ with diphenylsilane (Ph₂SiH₂), in the presence of excess PPh₃, results in the formation of [(Ph₃P)CuH]₆ in high yield.^{31,51} The failure to observe a Cu(0) nanocluster in this reaction can be rationalized on the basis of the higher stability of copper hydrides versus silver and gold hydrides. However, we hypothesized that performing the reduction of a Cu(I) salt in a ligand-deficient environment would result in the formation of unstable Cu_{*x*}H_{*x*} oligomers that could be more amenable to nanocluster growth. Thus, addition of 13 equiv of Ph₂SiH₂ to a slurry containing 24 equiv of Cu(OAc), 1 equiv of CuCl, and 12 equiv of PPh₃, in C₆H₆ results in a rapid color change from pale green to dark red. With further stirring, this solution undergoes a color change to deep green, concomitant with the deposition of a dark brown solid. Workup of this mixture after

Received: July 20, 2015

Published: September 30, 2015

Scheme 1. Synthesis of Complexes 1 and 2



14 h resulted in the isolation of two copper hydride clusters, $[\text{Cu}_{25}\text{H}_{22}(\text{PPh}_3)_{12}]\text{Cl}$ (**1**) and $[\text{Cu}_{18}\text{H}_{17}(\text{PPh}_3)_{10}]\text{Cl}$ (**2**), in isolated yields of 23% and 14%, respectively (Scheme 1). An insoluble dark brown powder was also isolated, which was subsequently identified to be elemental Cu (17% yield). Complexes **1** and **2** were separated on the basis of their different solubilities in C_6H_6 . Briefly, the reaction mixture was first crystallized from a CH_2Cl_2 /hexanes solution. This resulted in deposition of a mixture of dark-green (**1**) and yellow (**2**) crystalline materials. Extraction of these solids into C_6H_6 resulted in selective dissolution of **2**, which permitted its separation from **1** by filtration. Complex **1** was then extracted into CH_2Cl_2 and crystallized from CH_2Cl_2 /hexanes, while complex **2** was crystallized separately from C_6H_6 / CH_2Cl_2 / Et_2O . No doubt, this procedure contributed somewhat to the low isolated yields of **1** and **2**, as both are probably present in higher yields in the crude reaction mixture. The isolation of two different CuH clusters from the reaction can be rationalized by their similar Cu:P ratios (that of complex **1** is 2.1:1, while that of complex **2** is 1.8:1), both of which are similar to the Cu:P ratio in the original reaction mixture (2.1:1). Alternatively, the presence of both **1** and **2** in the reaction mixture suggests that they have similar thermodynamic stabilities. Interestingly, tractable material cannot be isolated without addition of 1 equiv of CuCl to the reaction mixture, which functions as a Cl^- source. Previously, we elucidated the significance of providing a counteranion source in the reaction mixture during CuH cluster synthesis.³¹ Importantly, while Ph_2SiH_2 reacts with Cu(OAc) , it is unable to reduce CuCl (see the Supporting Information for more details). This orthogonal reactivity permits the two copper salts to play different roles in the reaction.

To better understand the formation of **1** and **2**, we followed the reaction by ^1H and ^{31}P NMR spectroscopies. A ^1H NMR spectrum of the reaction mixture in C_6D_6 , after 18 h, reveals the presence of complexes **1** and **2**, as evidenced by the distinctive chemical shifts of their hydride ligands (Figure S17). In addition, this spectrum also revealed the presence of H_2 , which is likely generated during the formation of both complex **1** and bulk Cu metal. The presence of **1** and **2** in the reaction mixture is also supported by the in situ ^{31}P NMR spectrum (Figure S18a). In addition, a few other copper-containing species are also present in the reaction mixture, as evidenced by singlets at 4.15, -2.62, -4.57, and -6.06 ppm in this spectrum (Figure S18a). While these species have eluded isolation thus far, it is important to note that they are present as minor components of the reaction mixture. Nonetheless, the presence of these other copper-containing complexes in the reaction mixture also helps to account for the low isolated yields of **1** and **2**.

Complex **1** crystallizes in the orthorhombic space group $Pbca$ as a hexanes and dichloromethane solvate, $1 \cdot 4\text{C}_6\text{H}_{14} \cdot 0.5\text{CH}_2\text{Cl}_2$ (Figure 1). In the solid state, **1** features a central core of 13 Cu atoms arranged in a distorted centered-icosahedron. The central Cu atom features a coordination number of 12, identical to that observed in bulk Cu metal.⁵² An icosahedral Cu_{13} core is predicted computationally in metallic nanoclusters of intermediate size, although it differs from the *fcc* structure of

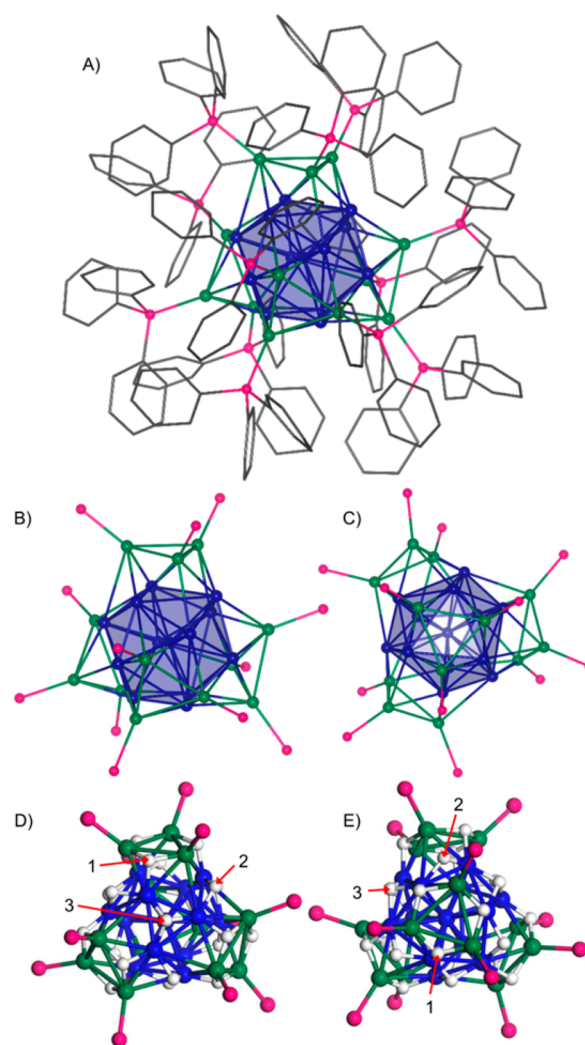


Figure 1. Ball and stick diagrams of **1**. The Cu_{13} centered-icosahedral core is highlighted in blue. The four $[\text{Cu}(\text{PPh}_3)_3]$ capping motifs are shown with the Cu atoms in green and P atoms in pink. (A) Side view with carbon atoms depicted in wireframe. All hydrogen atoms, chloride counterion, and solvent molecules have been omitted for clarity. (B) Side view showing only the Cu and P atoms. (C) Top view, looking down the C_3 axis, showing only the Cu and P atoms. (D and E) DFT-calculated structure, optimized using the PW91 functional. Two views of the cluster are shown to facilitate visualization of the hydride ligand positions. Labels 1, 2, and 3 indicate one of the 12 equivalent μ_3 -hydrides, one of six equivalent μ_4 -hydrides, and one of the four equivalent μ_3 -hydrides, respectively.

the bulk metal.⁵³ The Cu_{13} core is connected, via Cu–Cu bonds, to four triangular $[\text{Cu}(\text{PPh}_3)_3]$ motifs, which cap the icosahedron in a tetrahedral arrangement. As a result, the cluster occupies the high symmetry T point group. The Cu–Cu distances in **1** exhibit a large range (2.389(3)–3.037(3) Å), consistent with the diverse range of Cu coordination environments. The average $\text{Cu}_{\text{center}}\text{--Cu}_{\text{icos}}$ bond length (2.635 Å; range: 2.598(3)–2.663(3) Å) is longer than that observed for Cu metal (2.55 Å),⁵² but is comparable to those found in other Cu hydride clusters, such as $[\text{CuH}(\text{PPh}_3)_6]$ (av 2.630 Å),⁵⁴ $[(\text{Me}_3\text{-tach})_3\text{Cu}_6(\mu_6\text{-H})\text{Cl}_4]^{2+}$ (av 2.580 Å),⁵⁵ and the outer Cu–Cu distances in $[\text{Cu}_{20}\text{H}_{11}(\text{S}_2\text{P}(\text{O}^i\text{Pr})_2)_9]$ (2.5284(9)–2.7542(7) Å).³³ More importantly, the Cu_{13} core in **1** is similar to M_{13} icosahedral cores found in $[\text{Au}_{25}(\text{SCH}_2\text{CH}_2\text{Ph})_{18}]^-$,^{10,11} $[\text{Ag}_{21}(\text{S}_2\text{P}(\text{O}^i\text{Pr})_2)_{12}]^+$,⁹ and

$[\text{Au}_{13}(\text{PMe}_2\text{Ph})_{10}(\text{Cl})_2]^{3+}$,⁵⁶ demonstrating for the first time that structurally similar nanoclusters are isolable for all three coinage metals. Finally, the Cu–P distances (av 2.26 Å) are typical of those found in Cu(I) phosphine complexes,^{54,57} while the outer-sphere Cl^- counterion was found to be disordered over two positions.

Consistent with the high symmetry observed in the solid state, complex **1** features a single resonance in its $^{31}\text{P}\{^1\text{H}\}$ NMR spectrum, at -2.96 ppm in CD_2Cl_2 . The ^1H NMR spectrum of **1** features three broad resonances at -0.92 , 1.55 , and 2.07 ppm, which integrate for 4H, 12H, and 6H, respectively, and are assignable to 22 hydride ligands in three different chemical environments. Interestingly, the ^{31}P NMR spectrum of **1** in C_6D_6 features many more resonances than the spectrum recorded in CD_2Cl_2 (Figure S5). To explain this observation, we suggest that its Cl^- counterion forms a contact ion pair in this nonpolar solvent, breaking the symmetry of the cluster. Importantly, this transformation is reversible: recovery of this NMR sample and dissolution in CD_2Cl_2 regenerates the high symmetry structure (Figure S23). Complex **1** features a signal at m/z 4758.61 in its electrospray ionization (ESI) mass spectrum (see Supporting Information), which corresponds to the parent $[\text{M}]^+$ ion (calcd m/z 4758.50). Synthesis and characterization of the deuteride analogue, **1-d₂₂**, further supports our proposed formulation. As anticipated, complex **1-d₂₂** features singlets at -0.90 , 1.65 , and 2.11 ppm in its ^2H NMR spectrum, in a 4:12:6 ratio, respectively. In addition, complex **1-d₂₂** features a signal at m/z 4780.68 in its ESI mass spectrum, which corresponds to the $[\text{M}]^+$ parent ion (calcd m/z 4780.64), a shift of 22 m/z versus the signal observed for **1-h₂₂**. Most importantly, with only 22 hydride ligands and one Cl^- counterion, two of the Cu atoms in complex **1** must have a formal Cu(0) oxidation state to maintain charge balance, making complex **1** the first Cu nanocluster with partial Cu(0) character. Alternately, complex **1** can be described as an $n^* = 2$ superatom with closed-shell 1S^2 configuration.²⁴ Notably, there are only two other $n^* = 2$ superatoms known, $\text{Ag}_{14}(\text{SC}_6\text{H}_3\text{F}_2)_{12}(\text{PPh}_3)_8$ and $\text{Ag}_{16}(\text{SC}_6\text{H}_3\text{F}_2)_{14}(\text{DPPE})_8$ (DPPE = 1,2-bis(diphenylphosphino)ethane).^{58–60}

Complex **2** crystallizes in the monoclinic space group $P2_1/c$, as a dichloromethane solvate, $2\cdot 4\text{CH}_2\text{Cl}_2$ (Figure 2). In the solid state, **2** features a square antiprism $[\text{Cu}_8\text{H}]^{7+}$ core, which is connected, via Cu–Cu bonds, to two axial $[\text{Cu}(\text{PPh}_3)]^+$ units and eight equatorial $[\text{Cu}(\text{PPh}_3)]^+$ units. As a result of this arrangement, the cluster occupies the D_{4d} point group. As was observed for **1**, the Cu–Cu bonds in **2** exhibit a large range (2.456(4)–3.044(6) Å). These values are comparable to those exhibited by other CuH clusters, such as $[\text{Cu}_{14}\text{H}_{12}(\text{phen})_6(\text{PPh}_3)_4]^{2+}$ (2.487(3)–2.915(3) Å)³¹ and $[\text{Cu}_{20}\text{H}_{11}(\text{S}_2\text{P}(\text{O}^i\text{Pr})_2)_9]$ (2.3079(7)–2.8595(7) Å).³³ For further comparison, the average Cu–Cu distance in **2** (2.639 Å) is intermediate to the Cu–Cu distances reported for solid $[\text{CuH}]_x$ (2.85 Å) and Cu metal (2.55 Å).^{52,61} The short (av 2.559 Å) and long (av 2.893 Å) edges of the square antiprism result in a large internal volume (19.0 Å³), which is occupied by an interstitial hydride ligand (see below). The Cu–P distances (av 2.24 Å) are similar to those of **1** and other Cu(I) phosphine complexes.^{54,57} As with complex **1**, the outer-sphere Cl^- counterion was observed to be disordered over two positions.

Complex **2** features two resonances in its $^{31}\text{P}\{^1\text{H}\}$ NMR spectrum at -7.41 and 0.04 ppm in CD_2Cl_2 , in a 1:4 ratio, respectively. These resonances are assigned to the two axial and eight equatorial PPh_3 ligands, respectively, and are consistent

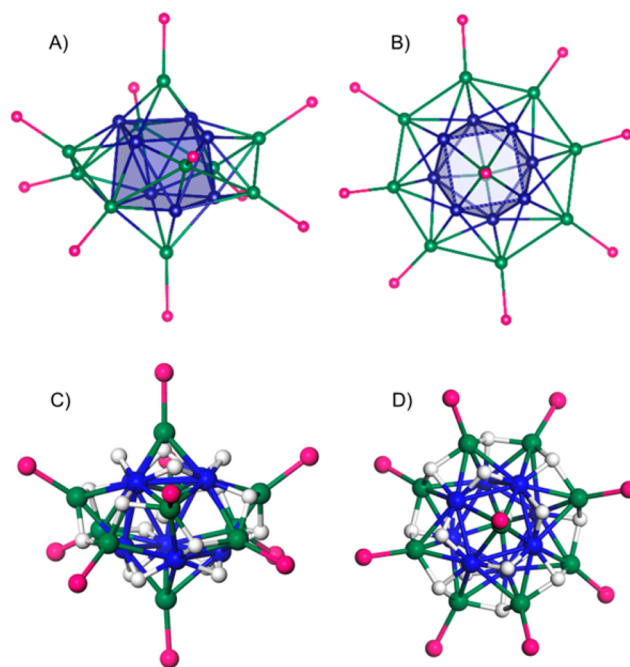
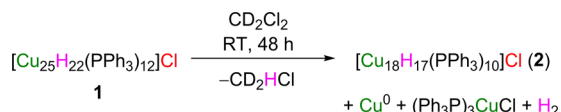


Figure 2. Ball and stick diagrams of **2**. The square antiprism Cu_8 core is highlighted in blue. The 10 $[\text{Cu}(\text{PPh}_3)]^+$ capping units are shown with the Cu atoms in green and P atoms in pink. The hydride ligands are shown in white. (A) Side view showing only the Cu and P atoms. (B) Top view, looking down the C_4 axis, showing only the Cu and P atoms. (C) Side view of calculated structure, optimized using the PW91 functional. (D) Top view of calculated structure, optimized using the PW91 functional.

with the high symmetry observed in the solid state. The ^1H NMR spectrum of **2** features three broad resonances at 1.17 , 2.74 , and 10.58 ppm, which integrate for 8H, 8H, and 1H, respectively. These are assignable to 17 hydride ligands in three different chemical environments. As was observed for complex **1**, the ^{31}P NMR spectrum of **2** in C_6D_6 features more resonances than its spectrum recorded in CD_2Cl_2 . In particular, seven resonances are observed, in a 2:2:2:1:1:1:1 ratio (Figure S12). This pattern can be rationalized by assuming that the Cl^- counterion binds to the cluster on a face defined by three equatorial phosphine ligands and one axial phosphine ligand. This interaction is likely quite weak, and probably promoted by the low dielectric constant of C_6D_6 . Notably, recovery of this NMR sample and dissolution in CD_2Cl_2 regenerates the high symmetry structure (Figure S25). Complex **2** features a signal at m/z 3783.80 in its ESI mass spectrum (see Supporting Information), which corresponds to the parent $[\text{M}]^+$ ion (calcd m/z 3783.78). Synthesis and characterization of the deuteride analogue, **2-d₁₇**, further supports these spectroscopic assignments. As anticipated, complex **2-d₁₇** features singlets at 1.25 , 2.79 , and 10.49 ppm in its ^2H NMR spectrum, in a 8:8:1 ratio, respectively. In addition, complex **2-d₁₇** features a signal at m/z 3800.95 in its ESI mass spectrum, which corresponds to the $[\text{M}]^+$ parent ion (calcd m/z 3800.88), a shift of 17 m/z versus the signal observed for **2-h₁₇**. Unlike complex **1**, with 17 hydride ligands and one Cl^- counterion, each Cu atom in **2** formally features a Cu(I) oxidation state assignment.

We also briefly probed the chemical properties of complexes **1** and **2**. Complex **1** is soluble in CH_2Cl_2 and THF, partially soluble in C_6H_6 and MeCN, and insoluble in Et_2O and nonpolar solvents. It is stable in THF for at least 3 d. However,

Scheme 2



it very slowly reacts with CD_2Cl_2 , generating complex 2, H_2 , copper metal, and $(\text{Ph}_3\text{P})_3\text{CuCl}$ (Scheme 2). These products are observed in the reaction mixture after 48 h, according to ^1H and ^{31}P NMR spectroscopies (Figures S19 and S20). We need to emphasize, however, that this is a very slow transformation, and even after 23 d, small amounts of complex 1 are still present in the NMR tube (see the Supporting Information for full details). We suggest that this reaction proceeds via hydride metathesis with the CD_2Cl_2 solvent, as was observed previously in the reaction of $[\text{Cu}_{14}\text{H}_{12}(\text{phen})_6(\text{PPh}_3)_4][\text{Cl}]_2$ with CD_2Cl_2 .³¹ Complex 2 is soluble in CH_2Cl_2 , partially soluble in C_6H_6 , THF, and MeCN, and insoluble in Et_2O and nonpolar solvents. Similar to 1, complex 2 very slowly reacts with CD_2Cl_2 , generating H_2 , copper metal, and $(\text{Ph}_3\text{P})_3\text{CuCl}$. Complex 1 is also formed in the reaction. These products are present in small amounts after 48 h, according to ^{31}P NMR spectroscopy (Figure S21). It should be noted, however, that even after 25 d, complex 2 is still the major component in the NMR sample. Thus, it appears that the stability of 2 in CD_2Cl_2 is significantly higher than that of complex 1.

To confirm our proposed formulations, and to predict the locations of the 22 hydride ligands in 1, as well as the 17 hydride ligands in 2, we explored their structures using density functional theory, as implemented in VASP 5.3.5.^{62–64} The interactions between valence electrons and atoms were described using the PAW method.⁶⁵ Both the PBE⁶⁶ and the PW91⁶⁷ exchange-correlation functionals were used to compare the predictions of different density functional approximations. Because of the large sizes of 1 and 2, only the Cu and hydride positions were allowed to relax during geometry optimization. A detailed description of the computational procedure is provided in the Supporting Information. The lowest energy structure for 1 is shown in Figure 1D and E. In this configuration, 12 equivalent hydride ligands are clustered into four groups of three. Each of these hydride ligands bridges two Cu atoms of a triangular $[\text{Cu}(\text{PPh}_3)_3]$ motif and one Cu atom belonging to the Cu_{13} icosahedron, in an overall μ_3 -coordination environment. The six equivalent hydride ligands exhibit asymmetric μ_4 -coordination, and are found along the six edges of the tetrahedron defined by the $[\text{Cu}(\text{PPh}_3)_3]$ motifs. For this environment, three of the Cu–H bond lengths are shorter (1.70–1.95 Å), whereas the fourth is much longer (2.3–2.5 Å). A similar asymmetry was observed for the μ_5 -H environment in $[\text{Cu}_{32}\text{H}_{20}\{\text{S}_2\text{P}(\text{O}^i\text{Pr})_2\}_{12}]$.³⁶ The four remaining hydride ligands bridge three equivalent Cu atoms belonging to the Cu_{13} icosahedron, in an overall μ_3 -coordination mode. Each of these hydride ligands is located directly opposite one of the four triangular $[\text{Cu}(\text{PPh}_3)_3]$ motifs. Overall, this 12:6:4 arrangement of hydrides is fully consistent with the NMR spectral data. Notably, this structure is calculated to be 0.4 eV lower in energy than the next most stable hydride conformation (the five lowest energy computed structures for 1 that obey the 12:6:4 hydride stoichiometry are shown in Figure S44).

The lowest energy computed structure for 2 is shown in Figure 2C and D. This structure features eight equivalent hydride ligands, each with a μ_3 -coordination mode, that reside

along the cluster's equator. Another eight hydride ligands are clustered into two groups of four. These hydride ligands also feature a μ_3 -coordination mode, and are located above and below the equatorial plane. The remaining hydride ligand is positioned within the square antiprism, and features a μ_4 -coordination mode, according to calculations. However, to account for the 8:8:1 arrangement of hydride ligands in the ^1H NMR spectrum, this interstitial hydride likely exhibits fluxional behavior, allowing it to coordinate equally to all eight Cu atoms of the square antiprism. Several alternate hydride positions were tested computationally for complex 2; however, none of these proved to be minima on the potential energy surface.

The Cu K-edge X-ray absorption near-edge spectrum (XANES) and extended X-ray absorption fine structure (EXAFS) were acquired, to probe the average oxidation state and coordination number of Cu in complex 1. The XANES in Figure 3 contains no pre-edge peaks, as appropriate for a cluster

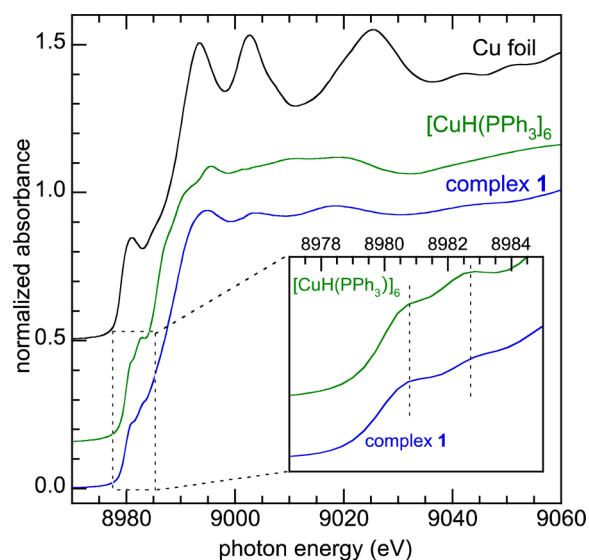


Figure 3. Comparison of the Cu K-edge XANES profile of complex 1 with those of $[\text{CuH}(\text{PPh}_3)_6]$ and Cu foil standards (vertically offset).

with a filled d-band. Nevertheless, the Cu K-edge is rich in structural information, due to the multiplicity of final states. The K_1 edge consists of two peaks, consistent with $4p_{xy}$ orbital degeneracy in the $[\text{CuP}(\mu_3\text{-H})_2]$ moieties, similar to $[\text{CuH}(\text{PPh}_3)_6]$.^{54,68} As expected, their intensities are attenuated in complex 1 due to the fractional contribution of such sites. At 8979.6 eV, the edge position of complex 1 lies between the values for Cu foil (8979.0 eV) and $[\text{CuH}(\text{PPh}_3)_6]$ (8980.0 eV) (Table 1). Considering the ca. 0.1 eV resolution of the spectrum, this is consistent with an average Cu oxidation state in the cluster that is intermediate between 0 and +1. While the

Table 1. Cu K-Edge Energies and Auger Parameters for Selected Cu(0) and Cu(I) Compounds

material	edge (eV)	Auger parameter (eV)
Cu foil	8979.0	1851.2 ⁷⁰
Cu nanoparticles (1–2 nm)	8979.0	1849.8–1850.8 ⁷¹
$[\text{Cu}_{25}\text{H}_{22}(\text{PPh}_3)_{12}][\text{Cl}]$ (1)	8979.6	1849.1
$[\text{CuH}(\text{PPh}_3)_6]$	8980.0	1848.6
$[\text{CuCl}(\text{PPh}_3)_4]$	8980.9	1847.4
CuCl	8981.9	1847.7

difference is small, it is notable that the edge energy of **1** is lower than that of $[\text{CuH}(\text{PPh}_3)]_6$, despite the much smaller ratio of PPh_3 ligands to Cu atoms in **1**. The P/Cu ratio is important because coordination of electron-donating PPh_3 to Cu affects the edge energy significantly. For example, the K-edge is shifted by 1.0 eV to lower energy in $[\text{CuCl}(\text{PPh}_3)]_4$, relative to CuCl (Table 1). The postedge oscillations characteristic of bulk Cu are strongly attenuated in **1**, as is typical of small Cu clusters, which lack long-range order.⁶⁹ The Cu Auger parameter, obtained from the XPS spectrum as the sum of the Cu $2p_{3/2}$ binding energy and the LMM Auger kinetic energy, can also be used to discriminate between Cu(I) and Cu(0), and is conveniently independent of XPS chemical shift calibration.⁷⁰ The value observed for **1** (1849.1 eV) lies between the Auger parameters recorded for $[\text{CuH}(\text{PPh}_3)]_6$ and Cu(0) (Table 1). This further supports our XANES K-edge energy assignment of complex **1** to an oxidation state intermediate between Cu(I) and Cu(0). The Cu:P ratio for **1**, as determined by XPS, also matches the predicted value (Table S4).

Curve-fitting of the Cu K-edge EXAFS was undertaken to explore the accuracy of the technique for determining the size of Cu NCs even in the absence of crystal structure data. The lack of appreciable long-range EXAFS intensity (beyond 3 Å) is consistent with the nanocluster formulation of **1**. A reasonable curvefit was obtained using a model with just two single-scattering paths: Cu–P and Cu–Cu. When the Cu–P degeneracy was fixed at 0.5, based on the known stoichiometry of the cluster, the Cu–Cu coordination number was refined to be (7.1 ± 0.9) . This is indistinguishable from the precise value for **1** (7.2), although the Cu–Cu path (2.52 Å) has a large mean-square displacement, 0.013 \AA^2 , reflecting the high variability in Cu–Cu nearest-neighbor distances (ranging from 2.39 to 3.04 Å, as described above). Because the EXAFS resolution is ca. 0.1 Å, this distance variability justifies the incorporation of another Cu–Cu single-scattering path. In the fit shown in Figure 4, the total Cu–Cu coordination number for both paths, (7.3 ± 1.2) , is also consistent with the known value. Thus, EXAFS analysis can provide reasonable

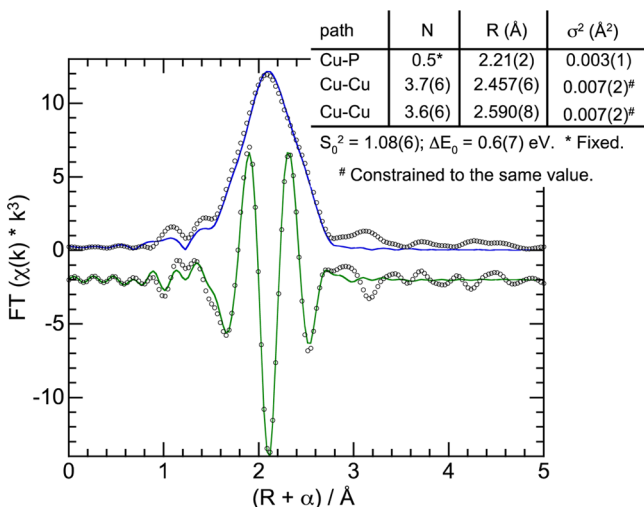


Figure 4. Cu K-edge EXAFS of complex **1** (points), in k^3 -weighted R -space (nonphase-corrected), showing curvefit to the magnitude (blue) and imaginary component (green) of the Fourier transform, as well as the curvefit parameters.

estimates of coordination number in monodisperse Cu systems, despite the inherent heterogeneity in Cu–Cu distances. Interestingly, both EXAFS pathlengths (2.46 and 2.59 Å) are located in the lower half of the $d(\text{Cu–Cu})$ range, consistent with the greater abundance of paths at these distances (Figure S1), as well as the greater signal attenuation expected for longer EXAFS paths.

SUMMARY

We have isolated and structurally characterized $[\text{Cu}_{25}\text{H}_{22}(\text{PPh}_3)_{12}]\text{Cl}$ (**1**), the first copper nanocluster with partial Cu(0) character. This material is built around a Cu_{13} centered-icosahedron, similar to the coordination environment observed in Cu metal (and in agreement with DFT-predicted structures for Cu clusters and nanoparticles). Moreover, the Cu K-edge XANES shows that **1** features an edge energy intermediate between those of Cu(0) and Cu(I). The Auger parameter recorded for **1** also falls between those measured for Cu(0) and Cu(I). Taken together, these data demonstrate for the first time that NCs with Cu(0) character are isolable for copper. Going forward, we suggest that **1** could function as a template for the synthesis of Cu NCs that are larger, and that contain greater Cu(0) character. Furthermore, **1** represents a unique opportunity to study the reactivity of Cu nanoclusters, and with this in mind we have begun exploring its reactivity toward a variety of small molecules, including CO_2 .

ASSOCIATED CONTENT

Supporting Information

The Supporting Information is available free of charge on the ACS Publications website at DOI: 10.1021/jacs.5b07574.

X-ray data for compound $1\cdot 4\text{C}_6\text{H}_{14}\cdot 0.5\text{CH}_2\text{Cl}_2$ (CIF)

X-ray data for compound $2\cdot 4\text{CH}_2\text{Cl}_2$ (CIF)

Experimental details, spectral data, and additional figures and tables (PDF)

AUTHOR INFORMATION

Corresponding Authors

*sscott@engineering.ucsb.edu

*hayton@chem.ucsb.edu

Notes

The authors declare no competing financial interest.

ACKNOWLEDGMENTS

This work was supported by the Center for Sustainable Use of Renewable Feedstocks (CenSURF), a National Science Foundation (NSF) Center for Chemical Innovation (CCI). The X-ray absorption spectroscopy studies were conducted on beam line 4-1, at the Stanford Synchrotron Radiation Lightsource, a Directorate of SLAC National Accelerator Laboratory and an Office of Science User Facility operated for the U.S. Department of Energy Office of Science by Stanford University. XPS studies were conducted at the MRL Shared Experimental Facilities, an MRSEC Program of the NSF (DMR 1121053).

REFERENCES

- Hakkinen, H. *Chem. Soc. Rev.* **2008**, *37*, 1847.
- Schmid, G. *Chem. Soc. Rev.* **2008**, *37*, 1909.
- Yamazoe, S.; Koyasu, K.; Tsukuda, T. *Acc. Chem. Res.* **2014**, *47*, 816.
- Li, G.; Jin, R. *Acc. Chem. Res.* **2013**, *46*, 1749.

- (5) Daniel, M.-C.; Astruc, D. *Chem. Rev.* **2004**, *104*, 293.
- (6) Parker, J. F.; Fields-Zinna, C. A.; Murray, R. W. *Acc. Chem. Res.* **2010**, *43*, 1289.
- (7) Harkness, K. M.; Tang, Y.; Dass, A.; Pan, J.; Kothalawala, N.; Reddy, V. J.; Cliffler, D. E.; Demeler, B.; Stellacci, F.; Bakr, O. M.; McLean, J. A. *Nanoscale* **2012**, *4*, 4269.
- (8) Desireddy, A.; Conn, B. E.; Guo, J.; Yoon, B.; Barnett, R. N.; Monahan, B. M.; Kirschbaum, K.; Griffith, W. P.; Whetten, R. L.; Landman, U.; Bigioni, T. P. *Nature* **2013**, *501*, 399.
- (9) Dhayal, R. S.; Liao, J.-H.; Liu, Y.-C.; Chiang, M.-H.; Kahlal, S.; Saillard, J.-Y.; Liu, C. W. *Angew. Chem., Int. Ed.* **2015**, *54*, 3702.
- (10) Heaven, M. W.; Dass, A.; White, P. S.; Holt, K. M.; Murray, R. W. *J. Am. Chem. Soc.* **2008**, *130*, 3754.
- (11) Zhu, M.; Aikens, C. M.; Hollander, F. J.; Schatz, G. C.; Jin, R. *J. Am. Chem. Soc.* **2008**, *130*, 5883.
- (12) Levi-Kalisman, Y.; Jadzinsky, P. D.; Kalisman, N.; Tsunoyama, H.; Tsukuda, T.; Bushnell, D. A.; Kornberg, R. D. *J. Am. Chem. Soc.* **2011**, *133*, 2976.
- (13) Jadzinsky, P. D.; Calero, G.; Ackerson, C. J.; Bushnell, D. A.; Kornberg, R. D. *Science* **2007**, *318*, 430.
- (14) Teo, B. K.; Keating, K. J. *J. Am. Chem. Soc.* **1984**, *106*, 2224.
- (15) Teo, B. K.; Hong, M.; Zhang, H.; Huang, D.; Shi, X. *J. Chem. Soc., Chem. Commun.* **1988**, 204.
- (16) Nunokawa, K.; Ito, M.; Sunahara, T.; Onaka, S.; Ozeki, T.; Chiba, H.; Funahashi, Y.; Masuda, H.; Yonezawa, T.; Nishihara, H.; Nakamoto, M.; Yamamoto, M. *Dalton Trans.* **2005**, 2726.
- (17) Yang, H.; Wang, Y.; Yan, J.; Chen, X.; Zhang, X.; Häkkinen, H.; Zheng, N. *J. Am. Chem. Soc.* **2014**, *136*, 7197.
- (18) Wang, Y.; Su, H.; Xu, C.; Li, G.; Gell, L.; Lin, S.; Tang, Z.; Häkkinen, H.; Zheng, N. *J. Am. Chem. Soc.* **2015**, *137*, 4324.
- (19) Yang, H.; Wang, Y.; Huang, H.; Gell, L.; Lehtovaara, L.; Malola, S.; Häkkinen, H.; Zheng, N. *Nat. Commun.* **2013**, *4*, 2422.
- (20) Yan, N.; Yuan, Y.; Dyson, P. J. *Dalton Trans.* **2013**, *42*, 13294.
- (21) Zhu, Y.; Qian, H.; Drake, B. A.; Jin, R. *Angew. Chem., Int. Ed.* **2010**, *49*, 1295.
- (22) Zhu, Y.; Qian, H.; Jin, R. *Chem. - Eur. J.* **2010**, *16*, 11455.
- (23) Zhu, Y.; Qian, H.; Jin, R. *J. Mater. Chem.* **2011**, *21*, 6793.
- (24) Walter, M.; Akola, J.; Lopez-Acevedo, O.; Jadzinsky, P. D.; Calero, G.; Ackerson, C. J.; Whetten, R. L.; Grönbeck, H.; Häkkinen, H. *Proc. Natl. Acad. Sci. U. S. A.* **2008**, *105*, 9157.
- (25) Wei, W.; Lu, Y.; Chen, W.; Chen, S. *J. Am. Chem. Soc.* **2011**, *133*, 2060.
- (26) Vilar-Vidal, N.; Rey, J. R.; López Quintela, M. A. *Small* **2014**, *10*, 3632.
- (27) Oyanagi, H.; Sun, Z. H.; Jiang, Y.; Uehara, M.; Nakamura, H.; Yamashita, K.; Orimoto, Y.; Zhang, L.; Lee, C.; Fukano, A.; Maeda, H. *J. Appl. Phys.* **2012**, *111*, 084315.
- (28) Oyanagi, H.; Orimoto, Y.; Hayakawa, K.; Hatada, K.; Sun, Z.; Zhang, L.; Yamashita, K.; Nakamura, H.; Uehara, M.; Fukano, A.; Maeda, H. *Sci. Rep.* **2014**, *4*, 7199.
- (29) Mazalova, V. L.; Soldatov, A. V.; Adam, S.; Yakovlev, A.; Möller, T.; Johnston, R. L. *J. Phys. Chem. C* **2009**, *113*, 9086.
- (30) Montano, P. A.; Shenoy, G. K.; Alp, E. E.; Schulze, W.; Urban, J. *Phys. Rev. Lett.* **1986**, *56*, 2076.
- (31) Nguyen, T.-A. D.; Goldsmith, B. R.; Zaman, H. T.; Wu, G.; Peters, B.; Hayton, T. W. *Chem. - Eur. J.* **2015**, *21*, 5341.
- (32) Huertos, M. A.; Cano, I.; Bandeira, N. A. G.; Benet-Buchholz, J.; Bo, C.; van Leeuwen, P. W. N. M. *Chem. - Eur. J.* **2014**, *20*, 16121.
- (33) Dhayal, R. S.; Liao, J.-H.; Lin, Y.-R.; Liao, P.-K.; Kahlal, S.; Saillard, J.-Y.; Liu, C. W. *J. Am. Chem. Soc.* **2013**, *135*, 4704.
- (34) Liao, J.-H.; Dhayal, R. S.; Wang, X.; Kahlal, S.; Saillard, J.-Y.; Liu, C. W. *Inorg. Chem.* **2014**, *53*, 11140.
- (35) Edwards, A. J.; Dhayal, R. S.; Liao, P.-K.; Liao, J.-H.; Chiang, M.-H.; Piltz, R. O.; Kahlal, S.; Saillard, J.-Y.; Liu, C. W. *Angew. Chem., Int. Ed.* **2014**, *53*, 7214.
- (36) Dhayal, R. S.; Liao, J. H.; Kahlal, S.; Wang, X.; Liu, Y. C.; Chiang, M. H.; van Zyl, W. E.; Saillard, J. Y.; Liu, C. W. *Chem. - Eur. J.* **2015**, *21*, 8369.
- (37) Moret, M.-E.; Zhang, L.; Peters, J. C. *J. Am. Chem. Soc.* **2013**, *135*, 3792.
- (38) Weinberger, D. S.; Amin Sk, N.; Mondal, K. C.; Melaimi, M.; Bertrand, G.; Stückl, A. C.; Roesky, H. W.; Dittrich, B.; Demeshko, S.; Schwederski, B.; Kaim, W.; Jerabek, P.; Frenking, G. *J. Am. Chem. Soc.* **2014**, *136*, 6235.
- (39) Jerabek, P.; Roesky, H. W.; Bertrand, G.; Frenking, G. *J. Am. Chem. Soc.* **2014**, *136*, 17123.
- (40) Ganesamoorthy, C.; Weßing, J.; Kroll, C.; Seidel, R. W.; Gemel, C.; Fischer, R. A. *Angew. Chem., Int. Ed.* **2014**, *53*, 7943.
- (41) Bratsch, S. G. *J. Phys. Chem. Ref. Data* **1989**, *18*, 1.
- (42) Li, C. W.; Ciston, J.; Kanan, M. W. *Nature* **2014**, *508*, 504.
- (43) Kas, R.; Kortlever, R.; Milbrat, A.; Koper, M. T. M.; Mul, G.; Baltrusaitis, J. *Phys. Chem. Chem. Phys.* **2014**, *16*, 12194.
- (44) Tang, W.; Peterson, A. A.; Varela, A. S.; Jovanov, Z. P.; Bech, L.; Durand, W. J.; Dahl, S.; Norskov, J. K.; Chorkendorff, I. *Phys. Chem. Chem. Phys.* **2012**, *14*, 76.
- (45) Li, C. W.; Kanan, M. W. *J. Am. Chem. Soc.* **2012**, *134*, 7231.
- (46) Qiao, J.; Jiang, P.; Liu, J.; Zhang, J. *Electrochem. Commun.* **2014**, *38*, 8.
- (47) Calle-Vallejo, F.; Koper, M. T. M. *Angew. Chem., Int. Ed.* **2013**, *52*, 7282.
- (48) Schouten, K. J. P.; Qin, Z.; Gallent, E. P.; Koper, M. T. M. *J. Am. Chem. Soc.* **2012**, *134*, 9864.
- (49) Churchill, M. R.; Bezman, S. A.; Osborn, J. A.; Wormald, J. J. *J. Am. Chem. Soc.* **1971**, *93*, 2063.
- (50) Albert, C. F.; Healy, P. C.; Kildea, J. D.; Raston, C. L.; Skelton, B. W.; White, A. H. *Inorg. Chem.* **1989**, *28*, 1300.
- (51) Lee, D.; Yun, J. *Tetrahedron Lett.* **2005**, *46*, 2037.
- (52) Wyckoff, R. W. G. *Crystal Structures*, 2nd ed.; Interscience Publishers: New York, 1963; Vol. 1.
- (53) Yang, M.; Jackson, K. A.; Koehler, C.; Frauenheim, T.; Jellinek, J. J. *Chem. Phys.* **2006**, *124*, 024308.
- (54) Bennett, E. L.; Murphy, P. J.; Imberti, S.; Parker, S. F. *Inorg. Chem.* **2014**, *53*, 2963.
- (55) Kohn, R. D.; Pan, Z.; Mahon, M. F.; Kociok-Kohn, G. *Chem. Commun.* **2003**, 1272.
- (56) Briant, C. E.; Theobald, B. R. C.; White, J. W.; Bell, L. K.; Mingos, D. M. P.; Welch, A. J. *J. Chem. Soc., Chem. Commun.* **1981**, 201.
- (57) Mao, Z.; Huang, J.-S.; Che, C.-M.; Zhu, N.; Leung, S. K.-Y.; Zhou, Z.-Y. *J. Am. Chem. Soc.* **2005**, *127*, 4562.
- (58) Gell, L.; Lehtovaara, L.; Häkkinen, H. *J. Phys. Chem. A* **2014**, *118*, 8351.
- (59) Yang, H.; Lei, J.; Wu, B.; Wang, Y.; Zhou, M.; Xia, A.; Zheng, L.; Zheng, N. *Chem. Commun.* **2013**, *49*, 300.
- (60) Yang, H.; Wang, Y.; Zheng, N. *Nanoscale* **2013**, *5*, 2674.
- (61) Goedkoop, J. A.; Andresen, A. F. *Acta Crystallogr.* **1955**, *8*, 118.
- (62) Kresse, G.; Furthmüller, J. *Comput. Mater. Sci.* **1996**, *6*, 15.
- (63) Kresse, G.; Furthmüller, J. *Phys. Rev. B: Condens. Matter Mater. Phys.* **1996**, *54*, 11169.
- (64) Kresse, G.; Hafner, J. *Phys. Rev. B: Condens. Matter Mater. Phys.* **1993**, *47*, 558.
- (65) Blöchl, P. E. *Phys. Rev. B: Condens. Matter Mater. Phys.* **1994**, *50*, 17953.
- (66) Perdew, J. P.; Burke, K.; Ernzerhof, M. *Phys. Rev. Lett.* **1996**, *77*, 3865.
- (67) Perdew, J. P.; Chevary, J. A.; Vosko, S. H.; Jackson, K. A.; Pederson, M. R.; Singh, D. J.; Fiolhais, C. *Phys. Rev. B: Condens. Matter Mater. Phys.* **1992**, *46*, 6671.
- (68) Hocking, R. K.; Solomon, E. I. In *Molecular Electronic Structures of Transition Metal Complexes I*; Mingos, D. M. P., Day, P., Dahl, J. P., Eds.; Springer: Berlin, Heidelberg, 2012; Vol. 142, p 155.
- (69) Bazin, D.; Rehr, J. J. *J. Phys. Chem. B* **2003**, *107*, 12398.
- (70) Wagner, C. D. *Faraday Discuss. Chem. Soc.* **1975**, *60*, 291.
- (71) de Crescenzi, M.; Diociaiuti, M.; Lozzi, L.; Picozzi, P.; Santucci, S.; Battistoni, C.; Mattogno, G. *Surf. Sci.* **1986**, *178*, 282.